crystals

MDPI

Review

A Modern Approach to HEAs: From Structure to Properties and Potential Applications

Radu Nartita [1], Daniela Ionita [1] and Ioana Demetrescu [1,2,*]

[1] Department of General Chemistry, Faculty of Chemical Engineering and Biotechnologies, National University of Science and Technology POLITEHNICA Bucharest, 313 Splaiul Independentei, 060042 Bucharest, Romania; radu_sorin.nartita@upb.ro (R.N.); daniela.ionita@upb.ro (D.I.)
[2] Academy of Romanian Scientists, 3 Ilfov Street, 050044 Bucharest, Romania
* Correspondence: ioana.demetrescu@upb.ro

Abstract: High-entropy alloys (HEAs) are advanced materials characterized by their unique and complex compositions. Characterized by a mixture of five or more elements in roughly equal atomic ratios, these alloys diverge from traditional alloy formulations that typically focus on one or two principal elements. This innovation has paved the way for subsequent studies that have expanded our understanding of HEAs, highlighting the role of high mixing entropy in stabilizing fewer phases than expected by traditional phase prediction methods like Gibbs's rule. In this review article, we trace the evolution of HEAs, discussing their synthesis, stability, and the influence of crystallographic structures on their properties. Additionally, we highlight the strength–ductility trade-off in HEAs and explore strategies to overcome this challenge. Moreover, we examine the diverse applications of HEAs in extreme conditions and their promise for future advancements in materials science.

Keywords: high-entropy alloys; advanced materials; multi-element alloys; HEA properties; HEA crystallographic structures; HEA applications

Citation: Nartita, R.; Ionita, D.; Demetrescu, I. A Modern Approach to HEAs: From Structure to Properties and Potential Applications. *Crystals* **2024**, *14*, 451. https://doi.org/10.3390/cryst14050451

Academic Editor: Shouxun Ji

Received: 23 April 2024
Revised: 4 May 2024
Accepted: 7 May 2024
Published: 9 May 2024

1. Introduction

High-entropy alloys (HEAs) have garnered significant attention in materials science due to their unique compositions and potential for exceptional mechanical properties [1–5]. These alloys, which consist of five or more elements in equal or nearly equal atomic ratios, were first conceptualized by Yeh et al. in Taiwan in 1995, introducing a new class of materials distinguished by their simple solid-solution phases—face-centered cubic (FCC) and body-centered cubic (BCC)—and potential for intermetallic compound formation [6].

However, the narrative traces the evolution of the field of HEAs, starting with the pioneering work of Cantor and his student Alain Vincent in 1981. They achieved a significant milestone by creating a multicomponent alloy composed of 20 different elements, each at 5 atomic percent. This alloy, despite being multiphase and brittle, exhibited fewer phases than predicted by Gibbs's phase rule, suggesting a deviation from traditional alloy behavior. Following this, Yeh and his team emphasized the role of high mixing entropy in reducing the number of phases and enhancing the properties of these alloys. They examined a range of equiatomic alloys, studying their microstructures, hardness, and corrosion resistance [7,8]. Their findings expanded the understanding of HEAs, demonstrating their complexity and the influence of factors like atomic size difference, valence electron concentration, and electronegativity on their formation, as outlined by Hume-Rothery's rules [6].

HEAs can be classified into seven primary families based on their constituent elements: 3d transition metals (including Cr, Ni, Fe, Mn, Cu, Al, Ti, V), which are the most extensively researched; refractory metals (Mo, Cr, Hf, Ti, Ta, Nb, W, V, Zr); lightweight metals (Mg, Al, Li, Be, Sn, Zn, Si, Ti, Sc); lanthanide (4f) transition metals (Gd, Dy, Tb, Lu, Tm, Y); brasses

and bronzes (Al, Cu, Mn, Ni, Sn, Zn); precious metals (Ag, Au, Co, Cr, Cu, Ni, Pd, Pt, Rh, Ru); and interstitial compounds (B, C, N). However, the immense compositional variety of HEAs means that some alloys do not neatly fit into these categories, demonstrating the field's complexity and the potential for innovative alloy design [7,9].

In this review article, we have employed a systematic approach to curate the most relevant and authoritative sources for the bibliography, considering the themes of the articles. The number of articles selected is illustrated in Figure 1.

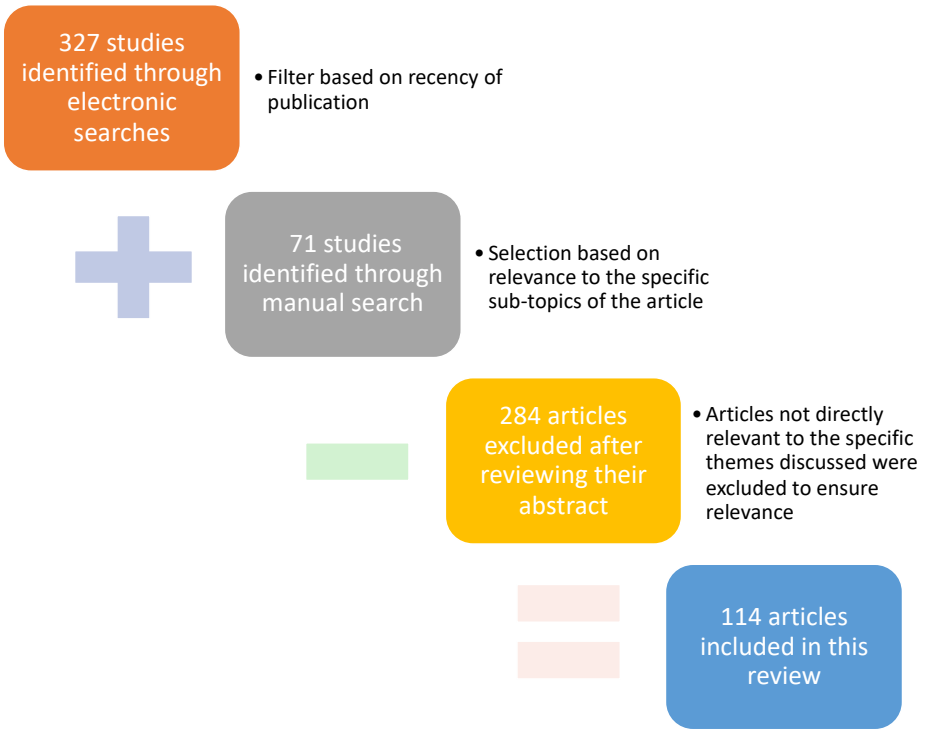

Figure 1. Article selection process.

Despite their promising attributes, HEAs encounter a significant challenge: the strength–ductility trade-off, which complicates their use as structural materials [10–13]. While single-phase FCC HEAs are celebrated for their ductility, they suffer from low tensile strength at room temperature. Conversely, BCC HEAs, despite their strength, are prone to early cracking and limited plasticity, undermining their malleability [14,15]. In the context of HEAs with an FCC crystal structure, the research primarily focuses on addressing the inherent trade-off between strength and ductility. Traditional methods like severe plastic deformation (via cold rolling or equal channel angular pressing) enhance strength at the cost of ductility, suggesting the possibility of developing superfunctional materials that surpass traditional engineering materials in performance [16]. This advancement points towards a future where HEAs could play a critical role in various high-efficiency, advanced material applications, demonstrating the field's growing maturity and potential for innovation [8,17,18].

Over the past decade, there has been a surge in HEA research, leading to the identification of promising single-phase HEAs, notably in FCC and BCC structures, with examples including $Fe_{20}Co_{30}Ni_{10}Cr_{20}Mn_{20}$ [19] and CoCrFeMnNi [20], and TiNbTaZrMoHfWCr [21], MoNbTiVTaW [22], and $Fe_{20}Mn_{15}Cr_{15}V_{10}Al_{10}C_{2.5}$ [23], respectively. These HEAs are not only simple in their crystal structures but also demonstrate exceptional mechanical strengths. Recent research has also expanded to understand the behavior of HEAs under different conditions, recognizing that these alloys can exhibit phase separation and ordering tendencies, influencing their microstructure and properties [24–26]. This shift acknowledges the dynamic nature of HEAs, which can present different phases depending on the temperature and other environmental factors [8]. In addition to mechanical and physical

properties, the scope of HEA research has broadened to include hydrogen storage [27], energy conversion [28], catalysis [29], and magnetic applications [30]. This diversification highlights the versatility and potential of HEAs in various fields. Regarding the countries most active in research on HEAs, Krishna et al. highlights that approximately 50% of the total number of publications originates from China, followed by the USA (11.2%), Germany (4.3%), India (3.9%), and Japan (3.1%) [7].

The uniqueness of HEAs lies within their mixed and uneven structure at the atomic level. Unlike conventional materials, which achieve unique properties through defect engineering to break their uniform energy landscapes, HEAs naturally possess these disrupted landscapes due to their chemically random makeup. This randomness comes from incorporating multiple elements in substantial proportions within the crystal lattice, diverging from traditional Hume-Rothery rules-based design. The resulting material showcases a vast diversity in atomic radii, electronegativities, valences, and magnetic moments, leading to unique nearest-neighbor environments and a highly distorted energy landscape characterized by uneven nearest-neighbor bond lengths and distorted charge densities [31]. To illustrate these complex interactions and their implications for the structural and physical properties of HEAs, Figure 2 provides a depiction of the core effects, further addressing the role of diverse atomic configurations in enhancing the materials' performance.

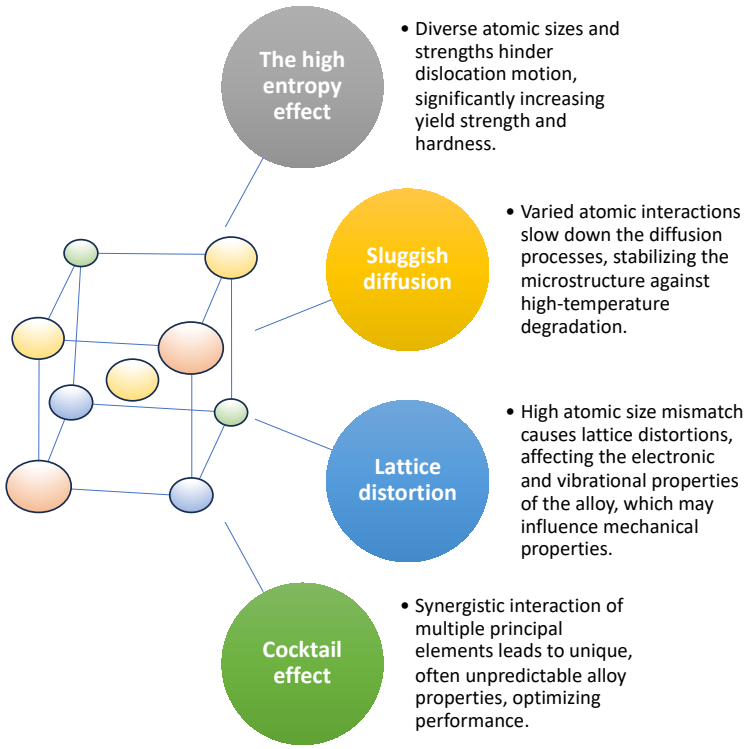

Figure 2. Core effects in HEAs and their influence on structure and properties.

2. Crystallographic Structures of High-Entropy Alloys

HEAs are renowned for their simple solid-solution phases, such as BCC, FCC, and hexagonal close-packed (HCP), which contrast with the complex and often more brittle structures of traditional alloys. The inherent high mixing entropy in HEAs not only simplifies their structure but also holds promise for a range of practical applications [7].

The exploration of HEAs has revealed a predominance of disordered FCC and BCC phases, with a comprehensive review conducted by Miracle and Senkov, which identified 408 unique alloys, expanding to 648 unique microstructure reports showing FCC and BCC phases observed 465 and 357 times, respectively. Despite this, the HCP structures, primarily composed of heavy rare-earth elements, are less common and under-researched in terms of their mechanical properties. The distribution of these phases demonstrates that FCC

structures are the most prevalent, found in 56% of instances, followed by BCC at 43%, and HCP structures are relatively rare, at 1% [9].

Recent research in HEAs has placed a focus on phase transformations, notably martensitic transformation, which facilitates rapid structural changes without diffusion, significantly affecting the mechanical behavior of these alloys [32]. Current strategies aim to harness the properties of single-phase, disordered solid-solution alloys and enhance them by leveraging metastability [33]. For example, altering the elemental content in certain alloys can destabilize the high-temperature FCC phase, inducing the transformation-induced plasticity (TRIP) effect, which, along with interface hardening and transformation hardening from dual-phase microstructures, has been effective in improving strength and ductility. This is particularly evident in HEAs like $Fe_{50}Mn_{30}Co_{10}Cr_{10}$, where optimizing the strength–ductility product index is a key goal [14]. Although structural components are designed to operate within the elastic regime under normal conditions, ductility can be important for safety reasons and resilience in structural applications, allowing materials to absorb energy and undergo significant deformation before failure, which is required in unexpected overloading or extreme conditions. Ductility also contributes to fatigue and fracture resistance, important under cyclic loading where ductile materials can withstand more stress cycles. Thus, ductility, alongside fracture toughness, plays a vital role in ensuring both performance and safety in engineering applications [34–36].

To navigate this strength–ductility conundrum, approaches like TRIP and twinning-induced plasticity (TWIP) are employed to introduce metastable phases and twinning boundaries, enhancing mechanical properties without compromising ductility [37]. Furthermore, the introduction of heterogeneous grain structures in HEAs creates domains of coarse and fine grains that experience varied plastic deformation levels, leading to significant strain gradients and hetero-deformation-induced (HDI) strengthening. This phenomenon allows for an increase in alloy strength while maintaining ductility [16]. In the development of a new class of lightweight metastable high-entropy alloys (LW metastable HEA), Yoon et al. utilized CALPHAD calculations to enhance the composition of traditional alloys, focusing particularly on achieving low-stacking-fault energy by increasing the fraction of lightweight elements among 3d transition metals. Systematic addition of aluminum (up to 5 atomic percent) to a base alloy of $Cr_{24}Mn_6Fe_{40}Co_{24}Ni_6$ led to significant changes in the crystallographic phases, transitioning from an initial dual phase of FCC and HCP to a single-phase FCC, and then to a dual phase of FCC and BCC, specifically a B2 phase. This evolution was crucial in achieving a balance of enhanced properties: the single-phase FCC structure notably exhibited a 10% reduction in density compared to the Cantor alloy, a threefold increase in lattice distortion leading to extremely low thermal conductivity, a 50% increase in the Hall–Petch coefficient, indicating solid-solution strengthening, and enabled complex deformation mechanisms like TRIP and TWIP, enhancing ductility over 40% [38]. These phase transformations underscore the pivotal role of crystallographic phases in tailoring the mechanical properties and performance of HEAs, providing a guideline for designing next-generation structural materials with optimized properties [38,39].

The ability to manipulate the phases, particularly to enhance the rare HCP structures or to exploit the TRIP effect, opens up new possibilities for developing advanced materials that could meet the demanding requirements of various structural applications. The B2 phase, enhanced by Co/Al addition, significantly increases the hardness of HEAs. Similarly, the presence of BCC-structured nanoprecipitates, encouraged by Fe/Mn addition, bolsters resistance to high-temperature softening and fracture, while also enhancing tribological properties. Mechanical alloying is vital for achieving homogeneous solid-solution strengthening, with Fe and Co additions limiting diffusion rates. The crystal structures, such as BCC, FCC, and HCP, are determined based on valence electron concentration (VEC) and affect the alloy's properties [40]. For instance, AlMgZnCuMn alloys exhibit stable solid solutions without excessive intermetallic compounds. The phase transition from BCC to FCC with increased mechanical alloying time and the addition of elements like Al in AlFeCuNiMgZn systems, is noted, indicating a link between processing conditions and

crystallographic phases. Moreover, the choice between BCC and FCC structures in an alloy system is influenced by VEC, with VEC < 6.87 indicating BCC and VEC > 8.6 indicating FCC. Additionally, the dual-phase structures, BCC + FCC, are of particular interest for their balanced properties, crucial for applications like turbine blades. Alloy systems like $Fe_{50}Mn_{30}Co_{10}Cr_{10}$ show a significant interplay between FCC and HCP phases, affecting grain boundary characteristics and area fractions. In dual-phase HEAs, such as Ni–Al, the B2 phase is pivotal for enhancing hardness and yield strength, while the Laves phase in Fe–Nb systems offers superior thermal stability. This complex interplay of crystallographic phases in HEAs underpins their tailored properties for specific applications [41].

A CrMnFeCoNi HEA with a single FCC phase was developed via hot rolling by Cheng et al. to achieve a mix of uncrystallized coarse grains and recrystallized fine grains. Dynamic compression tests at various temperatures provide insights into the temperature-dependent yield stress and strain hardening. Electron backscatter diffraction (EBSD) and transmission electron microscopy (TEM) analyses reveal that at lower temperatures, the alloy exhibits enhanced yield strength and strain hardening, attributed to nanoscale twinning induced by high-strain-rate deformation. The research contributes to the broader understanding of HEAs' crystallographic phases, particularly focusing on how the FCC structure's inherent ductility can be leveraged while overcoming its low-yield-strength limitations through innovative structural and deformation strategies [16].

One study conducted by Jian and Ren delves into the orientation-dependent tensile behaviors of the HfNbTaTiZr refractory high-entropy alloy using molecular dynamic simulations, aiming to enhance its application potential by understanding its mechanical responses. The findings reveal that the alloy's mechanical properties, such as Young's modulus and yield strength, are significantly influenced by its crystallographic orientation during uniaxial tension, with the [111] direction exhibiting the highest values. Moreover, the study identifies deformation mechanisms unique to specific orientations: a BCC–FCC phase transformation when tensile loading is along the [001] direction and a BCC–HCP transformation for [110] or [111] orientations. These insights underscore the importance of crystallographic orientation in tailoring the alloy's microstructure and mechanical performance, offering a pathway to optimize refractory high-entropy alloys for high-temperature and high-strain-rate applications [42].

Figure 3 provides a visualization of the structural characteristics of the various HEAs discussed throughout this article. It illustrates key structural differences and similarities among the types of HEAs, highlighting the unique crystallographic phases and microstructural elements that contribute to their remarkable properties.

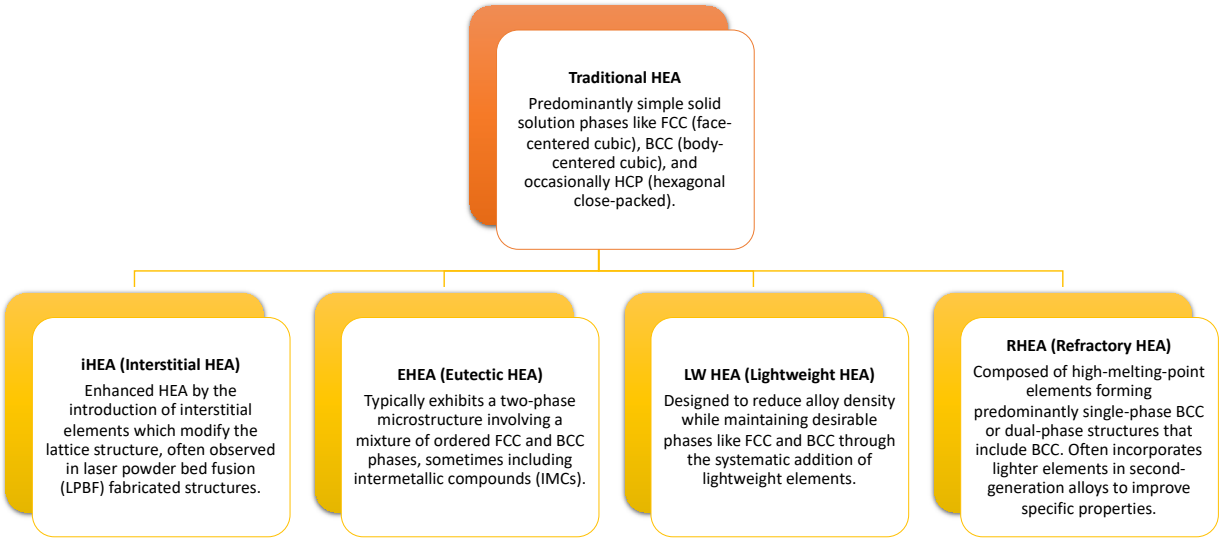

Figure 3. Structural characteristics of different types of HEAs.

3. Formation and Stability of High-Entropy Alloy Structures

HEAs inherently possess disrupted landscapes due to their chemically random structures, arising from the incorporation of multiple elements in significant proportions within their crystal lattice [43–45]. This deviation from the traditional Hume-Rothery rules leads to a material with a diverse array of atomic radii, electronegativities, valences, and magnetic moments, creating distinctive nearest-neighbor environments and a distorted energy landscape with irregular bond lengths and charge densities [31]. The role of enthalpy and coordination numbers in metallic systems is crucial for understanding HEA properties. Variations in coordination numbers, driven by atomic sizes and bonding energies, influence the enthalpy and consequently the alloy's stability and mechanical characteristics. In HEAs, these numbers deviate from those in pure metals, reflecting the complexity of bond formation and impacting the structural and mechanical traits of the alloys [9]. Several parameters have been proposed to predict the formation of solid solutions and the structure type [46]. The most used are presented below (c_i represents the atomic percentage, r_i the atomic radius, and VEC_i the valence electron concentration).

High mixing entropy:

$$\Delta S_{mix} = -R\sum c_i ln c_i, \tag{1}$$

where $\Delta S_{mix} > 1.5R$ for solid solution.

Atomic size difference:

$$\delta = 100\sqrt{\sum_{i=1}^{n} c_i\left(1 - \frac{c_i}{\left(\sum_{i=1}^{n} c_i r_i\right)^2}\right)} \tag{2}$$

where $\delta < 6.5\%$ for solid solution.

Valence electron concentration:

$$VEC = \sum_{1}^{n} c_i (VEC)_i \tag{3}$$

where $VEC > 8.6$ indicates FCC and $VEC < 6.87$ indicates BCC.

The synthesis of HEAs involves various techniques across solid, liquid, and gas states, each influencing the microstructure and properties of the alloys uniquely [6,47–55]. Solid-state methods [56], such as mechanical alloying and spark plasma sintering, combine materials below their melting points, enhancing microstructure and element diffusion. Liquid-state techniques [47,57], such as arc melting and laser cladding, melt elements before combination, reducing defects and achieving uniform compositions. Vapor-phase processes [58] like atomic layer deposition and molecular beam epitaxy provide precise control over composition and structure, pivotal for customizing HEA properties.

In the fabrication of HEAs, both processing and post-processing techniques are pivotal in determining their phase composition and microstructure, which in turn significantly influence their mechanical and physical properties. Solidification processes such as casting and additive manufacturing often result in heterogeneous microstructures due to varied cooling rates, which can be tailored for specific properties through controlled heat treatments such as annealing or tempering. Additionally, powder metallurgy offers unique opportunities for phase manipulation through selective sintering conditions. Post-processing techniques, including mechanical working and surface treatments, further refine these properties by inducing phase transformations and microstructural changes that enhance performance under specific operational conditions [7,14,59].

Further illustrating the potential of HEAs, research on an interstitial-strengthened HEA (iHEA) using laser powder bed fusion (LPBF) in additive manufacturing showcases the ability to produce materials with intricate geometries and enhanced mechanical properties. LPBF's process results in unique microstructures that significantly influence the material's mechanical behavior, evidenced by iHEA's high strength and ductility, making it suitable for demanding applications. In situ analysis and micropillar compression tests have revealed

the influence of crystallographic orientations on mechanical properties, highlighting the advanced capabilities of HEAs in materials science and engineering [60].

Moreover, in eutectic high-entropy alloys (EHEAs), the crystallographic structure plays a pivotal role in defining their exceptional mechanical properties [61–63]. These alloys, such as the $AlCoCrFeNi_{2.1}$ EHEA introduced by Lu et al., exhibit a unique eutectic microstructure that is not commonly found in traditional eutectic alloys. Typically, EHEAs present a two-phase structure resulting from the solidification process where the liquid phase transitions into two solid phases. This microstructure includes an ordered FCC phase, known as the $L1_2$ structure, and an ordered BCC phase, often the B2 structure. The FCC phase provides ductility due to its numerous slip systems, while the BCC phase enhances strength. Moreover, the presence of intermetallic compounds (IMCs) in the B phase, characterized by very negative mixing enthalpies and significant differences in atomic radii, contributes to the alloy's strength by forming hard and brittle IMCs. Conversely, the A phase, typically a solid solution with an FCC structure, benefits from the high-entropy effect, which reduces the electronegativity differences among elements, leading to a ductile solid-solution phase [64]. Zheng et el. confirms the findings of Lu et al. after the manufacturing of the $AlCoCrFeNi_{2.1}$ EHEA using selective laser melting (SLM) technology from pre-alloyed powders. The microstructure and mechanical properties of these as-printed alloys were thoroughly analyzed, revealing no significant defects like cracks or pores, and a very high relative density exceeding 99.5%. This indicates an excellent metallurgical bond between the melted layers. The microstructure of these as-printed EHEAs comprises FCC and B2 phases, displaying a distinctive "fish scale" pattern with ultrafine cellular and columnar structures and a preferred orientation. These microstructural features contribute to the alloys' mechanical performance, with the alloys exhibiting an ultimate tensile strength of 1159.4 MPa and an elongation at break of 29.0%. The superior mechanical properties are attributed to the ultrafine grains and the unique FCC–B2 core–shell structures developed during the SLM process. Furthermore, the study observed edge dislocations at the interfaces caused by thermal stress, which are impeded by the FCC–B2 core–shell structures, enhancing the ductility and strength of the material. This combination of features makes these EHEAs promising for applications requiring materials with high strength and ductility [65].

The microstructures of EHEAs are near equilibrium, featuring low-energy phase boundaries and stable dislocation structures, which contribute to their high fracture toughness and resistance to creep at elevated temperatures. Additionally, the fine solidification structure, a result of sluggish atomic diffusion, ranges from microns to tens of nanometers and enhances strength through grain boundary strengthening, effectively addressing the trade-off between strength and ductility. These crystallographic features underpin the superior mechanical properties of EHEAs, making them suitable for various advanced applications where materials are subjected to extreme conditions, such as in aerospace, nuclear, and marine engineering. The interplay of different crystallographic phases and their stability under diverse conditions are key to the alloys' performance, showcasing the critical role of crystallography in the design and application of advanced materials [64].

4. Properties of High-Entropy Alloys

The structural intricacy of HEAs plays a fundamental role in their unique attributes, including solid-solution strengthening, improved conductivities (both thermal and electronic), and enhanced irradiation resistance [66–69]. These properties are a consequence of the variability in lattice distortion, which varies with composition and crystallographic structure. The vast compositional range of HEAs presents myriad opportunities for materials design, capturing the attention of researchers focused on deciphering and leveraging the connection between lattice distortion and material attributes [31,70,71].

A pivotal study by Yin et al. underscores the significance of lattice distortion by examining the effects of adding vanadium to FCC and BCC alloy structures. The inclusion of vanadium, which has a distinct atomic radius compared to other elements in the alloy,

contributes to lattice misfit and consequently augments the mechanical properties. Specifically, the incorporation of V escalates misfit volumes, which correlates with enhancements in yield strength across various alloy systems. This finding underscores the potential of fine-tuning compositions in HEAs to induce specific lattice distortions, thereby achieving targeted material properties [31].

Building on previous studies of self-ordered oxide nanotubes on traditional alloys [72–74], Berger et al. explore the TiNbZrHfTa high-entropy alloy. They highlight its potential for orthopedic implant applications due to its unique crystallographic BCC structure, which consists of biocompatible, non-toxic refractory elements. This alloy combines high mechanical strength with a low Young's modulus, significantly reducing stress-shielding effects that often lead to bone resorption. Additionally, surface modifications such as anodization and pre-calcification enhance the alloy's bioactivity, promoting rapid hydroxyapatite deposition in simulated body fluids [75].

In another significant study, an examination of $AlNbTiZrSi_x$ high-entropy alloys in simulated seawater environments sheds light on their corrosion behavior and microstructural characteristics. As the silicon content increases, there is a noticeable reduction in grain size, potentially due to the precipitation of the Zr_5Al_3 phase, which refines the microstructure. However, this increase in silicon content appears to compromise the integrity of passive oxide films such as TiO_2, Nb_2O_5, and ZrO_2, diminishing the alloys' corrosion resistance in marine settings. Structurally, the alloys predominantly exhibit a BCC configuration with evidence of lattice distortion from the incorporation of zirconium and niobium, alongside indications of a secondary Zr_5Al_3 hexagonal phase, suggesting a complex dual-phase microstructure. This dual-phase structure plays a crucial role in determining the mechanical and corrosion properties of the alloys. Such investigations highlight the nuanced interplay between alloy composition and microstructure, providing crucial insights for optimizing HEA performance in specific environmental conditions [76].

Tunes et al. extend the HEA concept to high-entropy ceramics (HECs), specifically targeting applications in environments subjected to energetic particle irradiation. A novel high-entropy carbide within the quinary refractory system CrNbTaTiW was synthesized using magnetron sputtering. This material displayed nanocrystalline grains, a single-phase crystal structure, and a carbon content of approximately 50 atomic percent. To evaluate the irradiation response, the new carbide was subjected to heavy-ion irradiation while observing with in situ transmission electron microscopy at 573 K. The study also compared its behavior with an HEA in the same system. Remarkably, up to a dose of 10 displacements per atom, no displacement damage was observed in either the HEA or HEC. Furthermore, while xenon was implanted into both materials, causing bubble nucleation, the bubbles in the HEC were smaller than those in conventional nuclear materials [77]. This suggests that HECs, like their alloy counterparts, may be promising materials for nuclear energy applications due to their enhanced resistance to radiation-induced damage. When compared with HEA, HECs have shown improved irradiation resistance, as evidenced by fewer and smaller defects, which contribute to enhanced amorphization resistance and reduced volume swelling. Despite these positive attributes, a significant knowledge gap remains in understanding how the chemical complexity of HECs directly influences their observed material performance under irradiation in experimental settings [78].

In research conducted by Qi et al., molecular dynamic (MD) simulation is employed to investigate how crystallographic orientation influences the mechanical properties and microstructure evolution of a single-crystal CoCrFeMnNi high-entropy alloy with an FCC structure. This study is particularly focused on understanding these effects through nanoindentation techniques. Initially, the research validates the MD simulation results at the elastic stage of the load–displacement (P–h) curve by comparing them with the Hertz contact theory, establishing the accuracy of the simulations. During the plastic deformation phase, the study examines the relationship between the P–h curve and the instant defect structure, finding that plastic deformation is primarily governed by the nucleation of Shockley partial dislocations or the movement of stacking faults. The study

delves deeper into the impact of crystallographic orientations ([001], [110], and [111]) on the mechanical response and microstructure evolution of the material. It finds that these orientations significantly influence the slip mode and stress concentration areas. Notably, a distinct "pop-in" behavior, indicative of sudden material displacement, is observed in the [111]-oriented sample but not in others, highlighting the orientation-dependent mechanical response. Microstructure evolution is shown to be anisotropic across different crystallographic orientations, leading to variations in dislocation density and hardness. The research establishes a linear relationship between the square root of dislocation density and hardness, aligning well with the Taylor hardening expression, which indicates that the hardening factor is highly dependent on the crystallographic orientation. This study's findings underscore the predictive compatibility between classical continuum mechanical theories and atomistic MD simulations, reinforcing the utility of these theories in interpreting and predicting the behavior of materials at the atomic scale. The insights into how crystallographic orientations affect material properties at the microstructural level are vital for the design and development of new materials with tailored mechanical properties [79].

Another study employs nonequilibrium molecular dynamic simulations to investigate the shock-induced plasticity in an FCC CoCrFeMnNi HEA and how it varies with crystallographic orientation. The research specifically focuses on the local transitions from FCC to BCC structures under shock loading and how these transitions influence plastic deformation. When shock loading is applied along the [001] direction, a local transition from the FCC to the BCC structure is observed. This transition is attributed to the compression along the <001> direction in the original body-centered tetragonal (BCT) structure, which subsequently encourages dislocation nucleation within the BCC structures. These dislocations then slip, leading to the formation of hexagonal close-packed (HCP) structures within the FCC lattice. Conversely, when shock loading is applied along the [110] and [111] directions, the study finds a prevalence of disordered structures. This outcome is linked to inadequate lattice displacement along the <112> direction on the {111} crystal plane of the FCC structure and a lack of coordinated deformation among the <001>, <110>, and <111> directions in the BCT structure. Notably, the presence of BCC and disordered structures, particularly those with Mn-rich compositions, is crucial for fostering localized plastic deformation. This phenomenon is associated with stress concentration around Mn atoms, stemming from the alloy's inherent local inhomogeneity. Moreover, under shock loading, the elevated atomic fraction of local BCC and disordered structures contribute to increased chemical composition heterogeneity within these areas. These findings offer valuable insights into the mechanisms of shock-induced plasticity in CoCrFeMnNi HEAs, highlighting the significant role of crystallographic orientation in dictating the material's response to shock loading. This research contributes to a deeper understanding of plastic deformation in HEAs under extreme conditions, which is vital for designing materials with optimized resistance to shock and other dynamic stresses [80].

When comparing the performance of high-entropy alloys to that of traditional alloys, performance indices can be an excellent tool. These performance indices are derived from basic engineering principles and are used to quantitatively assess the suitability of different materials for specific applications. The process involves plotting these indices on charts, which visually represent the trade-offs and capabilities of various materials, allowing quick identification of the materials that fall within the desired performance range. By incorporating considerations for both material properties and geometric design factors (such as the shape of the component), performance indices facilitate a holistic approach to engineering design. This approach ensures that all aspects of performance, including mechanical strength, weight, and cost, are balanced to meet the specific requirements of the application [81,82].

Figure 4 illustrates how each HEA type uniquely contributes to enhanced performance metrics such as strength, ductility, corrosion resistance, and thermal stability, providing a clear comparative perspective.

Figure 4. Properties of different types of HEAs.

5. Applications of High-Entropy Alloys in Extreme Conditions

Some HEAs have enhanced thermal conductivity, which can significantly improve heat transfer efficiency in nuclear reactor components. They combine exceptional mechanical properties like high tensile strength, flexibility, and hardness, making them suitable for various nuclear applications, including reactor pressure vessels and fuel cladding. HEAs maintain structural integrity under extreme temperatures and show excellent resistance to creep, making them ideal for high-temperature nuclear reactor environments [83–85]. Additionally, HEAs offer superior resistance to radiation-induced damage compared to conventional alloys, due to their unique atomic structures and high configurational entropy, enhancing their long-term durability in nuclear reactors [86,87]. Refractory metal-based complex concentrated alloys (RCCAs), including refractory high-entropy alloys (RHEAs), represent significant advancements in materials science, offering a unique blend of properties ideal for high-temperature applications [2,88,89]. HEAs are noted for their stability, hardness, ductility, strength, and resistance to various forms of degradation, making them suitable for harsh environment applications. Specifically, RCCAs and RHEAs are distinguished by their ability to maintain strength at temperatures substantially higher than Ni-based superalloys, with some maintaining mechanical integrity up to about 0.6–0.7 times their absolute melting temperature. These alloys, especially those with higher melting points,

exhibit effective strength within a considerable temperature range, such as 1363–1941 K (1090–1668 °C), depending on their melting point thresholds [90–92].

The microstructure of RCCAs, often dominated by a single-phase BCC or multiphase structures with BCC prevalence, contributes to their broad range of compositions, densities, and oxidation resistance, surpassing traditional refractory materials [93]. However, this also implies a possible ductile-to-brittle transition temperature (DBTT) above room temperature, affecting their fracture behavior. The DBTT, alongside the temperature-dependent yield and fracture strength, indicates the complex interplay between temperature and mechanical properties in these alloys. Furthermore, the room temperature tensile properties of RCCAs, such as the HfNbTaTiZr alloy, are intricately linked to their microstructure, interstitial elements, and processing history, highlighting the sensitivity of their mechanical characteristics to these factors. Disparities in tensile properties reported by different research groups underline the challenge in standardizing and predicting the behavior of RCCAs, emphasizing the need for a thorough understanding of their microstructural and compositional intricacies to harness their full potential in high-temperature applications [91].

The first-generation NbMoTaW series alloys showcased impressive yield strength at elevated temperatures, but were hindered by low ductility and high density. This prompted the development of second-generation RHEAs, where heavier elements like W, Mo, and Ta were substituted with lighter ones such as Ti, V, Zr, and Cr to enhance specific properties. Second-generation RHEAs, particularly those incorporating Al or Si, exhibit reduced densities compared to their predecessors, with some alloys demonstrating densities below 7 g/cm^3 [94]. While reduced density is not necessarily a requirement of the materials used in refractory applications, it can often be advantageous in applications such as jet engines and turbines [95]. For instance, the $Ti_{67}Nb_{16}Zr_{17}Al_{13}$ alloy displays an impressive combination of strength and ductility, indicative of the advancements in RHEA design. Several studies have delved into these alloys' microstructural and mechanical behaviors. For example, the presence of Al leads to a mixture of continuous B2 and disordered BCC phases, with the B2 phase's ductility being adjustable through the addition of specific elements. This dual-phase structure, particularly after specific heat treatments, shows enhanced mechanical properties at room temperature. Notably, the addition of Al not only reduces the overall density of the alloys but also contributes to their mechanical strengthening through second-phase strengthening and lattice distortion. However, there is a trade-off, as increased Al content has been observed to decrease plasticity while boosting compressive strength. These findings underline the complex interplay between alloy composition, microstructure, and mechanical properties, emphasizing the necessity for a nuanced approach in RHEA design and optimization to harness their full potential for high-temperature and high-stress applications [94].

Wang et al. delve into the development and analysis of second-generation non-isoatomic RHEAs, specifically the $NbTa_{0.5}Ti\text{-}Al_x$ series, fabricated through arc melting. These alloys are part of an evolving category of RHEAs designed to mitigate the limitations of first-generation RHEAs, such as their low ductility and high density, by incorporating lighter elements like Al, which not only reduce density but also influence the alloy's phase structure and mechanical properties. The $NbTa_{0.5}Ti\text{-}Al_x$ series demonstrates a transition from a single-phase BCC structure to a dual-phase A2 + B2 crystal structure with the addition of aluminum. This transformation is pivotal, as it leads to a significant enhancement in the alloy's hardness and strength, attributed to solution strengthening and precipitation strengthening effects. However, this increase in strength is accompanied by a rise in brittleness. Upon annealing, the alloys exhibit the formation of Laves-phase $NbAlTi_2$ and A15-phase $AlTi_3$ precipitates, which are crucial for the material's mechanical properties. These precipitates, varying in morphology from plate-like to needle- or particle-like, predominantly form at or near grain boundaries, influencing the alloy's overall mechanical behavior. The study also highlights the importance of annealing temperature, which aids in the dissolution of dendrites caused by elemental segregation during the cooling process post-arc melting, and promotes grain growth, enhancing the material's microstructural

characteristics. This research underscores the complexity of tailoring RHEAs' properties through compositional adjustments and thermal processing, offering insights into the potential of these advanced materials for applications requiring a balance of strength, ductility, and reduced density at elevated temperatures [94].

CoCrNiFeMn alloys, commonly known as Cantor alloys, and their derivatives are renowned for their excellent synergy of strength and ductility across a broad temperature spectrum, making them prime candidates for use in harsh environments. This performance is attributed to their low-stacking-fault energy, which facilitates deformation twinning and the TRIP effect under external strain. However, the inherent low strength and high malleability associated with the FCC structure of CoCrNi-based HEAs or medium-entropy alloys (MEAs) can lead to detrimental microstructural changes under extreme stress or wear conditions, adversely affecting their strength and wear resistance. Investigations on the microstructure of sintered $(CoCrNi)_{94}Ti_3Al_3$ MEA composites show a single FCC structure, as confirmed by X-ray diffraction (XRD) patterns and scanning electron microscopy with backscattered electron (SEM-BSE) imaging. The introduction of Al_2O_3 nanoparticles into the MEA results in a decrease in peak intensity in the XRD patterns, likely due to the high surface energy of the nanoparticles, which promotes their integration into the alloy powder. Notably, this addition does not introduce new ceramic or intermetallic phases, indicating good chemical stability between the alloy and the nanoparticles. Further observations reveal that increasing the concentration of Al_2O_3 nanoparticles leads to a higher surface content of these particles in the composite, with some agglomeration noted at higher concentrations. This research underscores the potential of nano-oxide reinforcement in enhancing the properties of CoCrNi-based alloys, potentially offsetting their intrinsic weaknesses under severe operational conditions [96]. Table 1 summarizes the potential applications of HEAs, showcasing how these materials excel in environments that demand high mechanical strength, superior thermal stability, and exceptional resistance to wear and corrosion. This table highlights specific use cases, such as in aerospace, nuclear energy, and high-temperature industrial processes, demonstrating the critical roles HEAs can play across various demanding sectors.

Table 1. Potential applications of HEAs in demanding conditions.

Application	HEA Type	Key Performance Metrics	Reference
Nuclear reactor components	General HEAs	Enhanced thermal conductivity; resistance to creep; superior radiation damage resistance.	[86]
High-temperature aerospace applications	RCCAs and RHEAs	Maintain strength up to 0.6–0.7 times melting temp; operate effectively within 1363–1941 K.	[9,91,92]
High-stress turbine blades	Second-generation RHEAs	Balance of strength and ductility; Reduced density; strength maintained at elevated temperatures.	[94]
Automotive and aerospace structural components	Cantor alloys and derivatives	High synergy of strength and ductility across temperatures; low-stacking-fault energy-enhancing twinning and TRIP effect; overcoming the strength–ductility trade-off through innovative alloying and processing techniques.	[14,96]
Lightweight structural applications	Lightweight metastable HEAs (LMH)	Low density with high specific strength and large ductility; TRIP-assisted dual-phase stability.	[38]
High-performance coatings	Various HEA families (refractory, transition metals)	Improved wear and corrosion resistance, thermal stability; suitable for extreme conditions like aerospace engines.	[6,7]
Interfacial joining in manufacturing and aerospace	General HEAs	Improved wetting characteristics, high mechanical strength, excellent corrosion and oxidation resistance, suitable for high-temperature applications.	[90]
Corrosion resistance in marine environments	$AlNbTiZrSi_x$ HEAs	Corrosion resistance varies with Si content; passive films mainly consist of TiO_2, Nb_2O_5, and ZrO_2. Si addition generally decreases passive film stability and corrosion resistance, particularly in simulated seawater.	[76]

Table 1. *Cont.*

Application	HEA Type	Key Performance Metrics	Reference
Ultralong-life fatigue resistance in structural components	CoCrFeMnNi (single-phase FCC equiatomic)	Exceptional very high cycle fatigue regime performance up to 10^9 cycles, high strength and ductility, sensitivity to microstructural control and casting defects.	[97]
Applications requiring enhanced wear resistance and hardness	$AlCoCrFeNiTi_{0.2}$	Enhanced hardness and wear resistance post-nitrogen ion implantation; phase transformation from r to BCC; increased hardness-to-Young's modulus ratio, suggesting improved resistance to mechanical wear and cracking.	[98]
Extreme environment applications	Refractory amorphous high-entropy alloys (RAHEAs)	Enhanced phase stability under extreme conditions; excellent performance under high-temperature annealing and irradiation; potential self-healing properties through nanoprecipitate reassembly enhancing radiation resistance.	[92]

6. Future Directions

The journey of HEAs through generations of development encapsulates their transformative evolution within materials science. Initially, the focus was on first-generation HEAs, which primarily utilized single-phase FCC and BCC structures. These alloys typically incorporated 3d transition and refractory metals, laying the groundwork for basic high-entropy alloy frameworks. Over time, the field has shifted towards more sophisticated second-generation alloys, which are characterized by complex, multiphase microstructures that not only enhance the material properties but also broaden the potential applications of HEAs [99–103].

In this new generation, the design strategies have become more nuanced, incorporating specific adjustments in alloy chemistry. These modifications aim to initiate mechanisms such as induced plasticity effects, which are particularly beneficial under mechanical stress conditions. Furthermore, these strategies encourage the formation of secondary strengthening phases, such as the $L1_2$ phase, within FCC-based materials. The integration of these phases is intended to augment the mechanical strength and durability of the alloys, making them suitable for more strenuous applications [104–106]. A particularly significant advancement in the field is the development of BCC + B2 two-phase microstructures. Within these structures, B2 precipitates are dispersed throughout a BCC matrix. This arrangement significantly enhances the mechanical properties of the alloys, especially in terms of their strength and temperature resilience, making them highly effective for high-temperature applications ranging from 1200 to 1500 °C [107–109]. Such capabilities make these alloys ideal for critical applications in aerospace and power generation, where materials are required to perform reliably under extreme conditions.

To support and expedite these innovations, the materials science community has embraced a collaborative approach that leverages data mining alongside computational and experimental methods. This integration facilitates the rapid synthesis and testing of novel alloy compositions, thereby accelerating the pace of materials discovery and innovation. It allows for a more efficient exploration of the vast compositional landscape of HEAs, pinpointing optimal combinations of elements that meet specific performance criteria [45,110–114].

Thus, the evolution of HEAs from their inception as simple single-phase systems to complex, multiphase structures illustrates not only the growth of the field but also the increasing sophistication of the materials being developed. As research continues, these materials are poised to play a pivotal role in advancing a range of high-tech industries, driving forward the development of next-generation materials tailored for the most demanding of applications.

7. Conclusions

In this review, we have investigated the intricate landscape of HEAs, a growing field in materials science characterized by its radical departure from traditional alloy systems and

its exploration into the diverse potential of multi-element solutions. The examination of HEAs from their conceptual origins to their current sophisticated forms reveals a dynamic evolution driven by the interplay of complex crystallographic structures and advanced processing techniques. The insights into the strength–ductility trade-off, phase stability, and the transformative effects of mechanical and thermal treatments elucidate the profound impact of microstructural control on the performance of these alloys.

HEAs offer a promising avenue for the development of materials that can operate under extreme conditions, such as high temperatures, corrosive environments, and high stress, making them ideal candidates for applications ranging from aerospace to nuclear reactors. We identify several promising areas for future investigation, including the potential of HEAs in renewable energy applications, such as hydrogen storage and photovoltaic systems, where their exceptional properties could overcome the limitations of current materials. Additionally, the development of advanced manufacturing techniques, such as 3D printing of HEAs, opens up new avenues for complex, lightweight structural designs in aerospace and automotive industries.

As we look to the future, the continued exploration of HEAs will undoubtedly involve a deeper integration of computational modeling, experimental validation, and innovative alloy design strategies. This will enhance our capability to tailor materials with specific properties, paving the way for the creation of next-generation materials that combine exceptional performance with sustainability. The progress in this field will rely heavily on a multidisciplinary approach, blending insights from physics, chemistry, and engineering to overcome current limitations and unlock new possibilities in materials science. Future research should focus on exploiting these tools to accelerate the discovery of novel HEA compositions with tailored properties for specific industrial applications.

However, the path forward is not without challenges. The scalability of HEA production and the cost of raw materials remain significant challenges. Collaborative efforts between academia and industry are essential to address these challenges and to harness the full potential of HEAs. Interdisciplinary research combining insights from materials science, solid-state physics, and engineering will be crucial in overcoming these barriers and realizing the innovative applications of HEAs.

Author Contributions: Conceptualization, I.D.; methodology, I.D. and D.I.; investigation, R.N., D.I. and I.D.; writing—original draft preparation, R.N., D.I. and I.D.; writing—review and editing, I.D. and D.I.; visualization, R.N.; supervision, I.D. All authors have read and agreed to the published version of the manuscript.

Funding: This research was funded by the Executive Agency for Higher Education, Research, Development and Innovation Funding, grant PN-III-P2-2.1-PED-2021-2884 (605PED/2022).

Data Availability Statement: The original contributions presented in the study are included in the article.

Conflicts of Interest: The authors declare no conflicts of interest.

References

1. Liu, L.; Wang, Z.; Wu, Q.; Jia, Y.; Xu, Q.; He, F.; Li, J.; Wang, J. A hypoeutectic high-entropy alloy with hierarchical microstructure for high-temperature application. *Scr. Mater.* **2023**, *232*, 115502. [CrossRef]
2. Wan, Y.; Cheng, Y.; Chen, Y.; Zhang, Z.; Liu, Y.; Gong, H.; Shen, B.; Liang, X. A Nitride-Reinforced NbMoTaWHfN Refractory High-Entropy Alloy with Potential Ultra-High-Temperature Engineering Applications. *Engineering* **2023**, *30*, 110–120. [CrossRef]
3. Wu, S.; Tang, Y.; Gu, J.; Li, R.; Liang, Y.; Liu, P.; Wang, H.; An, C.; Deng, Q.; Zhao, L.; et al. Controllable preparation of metal-based lubrication coatings in extreme environmental applications. *Mater. Des.* **2024**, *241*, 112922. [CrossRef]
4. Dong, D.; Jiang, W.; Wang, X.; Ma, T.; Zhu, D.; Wang, Y.; Huo, J. Enhanced mechanical properties of high pressure solidified $CoCrFeNiMo_{0.3}$ high entropy alloy via nano-precipitated phase. *Intermetallics* **2024**, *166*, 108192. [CrossRef]
5. Fu, G.; Liu, X.; Yi, X.; Zhang, S.; Cao, X.; Meng, X.; Gao, Z.; Wang, H. Development of High-Entropy Shape-Memory Alloys: A Review. *Metals* **2023**, *13*, 1279. [CrossRef]
6. Wang, Y.; Zhang, J.; Wu, T.; Huang, G. An all-around way to analyze the corrosion behavior and the potential applications of high-entropy alloys coating. *Ceram. Int.* **2024**, *50*, 5893–5913. [CrossRef]

7. Krishna, S.A.; Noble, N.; Radhika, N.; Saleh, B. A comprehensive review on advances in high entropy alloys: Fabrication and surface modification methods, properties, applications, and future prospects. *J. Manuf. Process.* **2024**, *109*, 583–606. [CrossRef]
8. Naseri, M.; Moghadam, A.O.; Anandkumar, M.; Sudarsan, S.; Bodrov, E.; Samodurova, M.; Trofimov, E. Enhancing the mechanical properties of high-entropy alloys through severe plastic deformation: A review. *J. Alloy. Metall. Syst.* **2024**, *5*, 100054. [CrossRef]
9. Miracle, D.B.; Senkov, O.N. A critical review of high entropy alloys and related concepts. *Acta Mater.* **2017**, *122*, 448–511. [CrossRef]
10. Ali, N.; Zhang, L.; Dongming, L.; Zhou, H.; Sanaullah, K.; Zhang, C.; Nian, Y.; Cheng, J. Enhancing the strength-ductility synergy in hot-forged $Fe_{50}Mn_{30}Co_{10}Cr_{10}$ high entropy alloy (HEA) through carbon additions. *J. Mater. Res. Technol.* **2024**, *29*, 5646–5655. [CrossRef]
11. Ojha, P.K.; Yoshida, S.; Sunkari, U.; Tripathy, B.; Tsuji, N.; Bhattacharjee, P.P. Highly deformable Laves phase in a high entropy alloy. *Scr. Mater.* **2024**, *240*, 115828. [CrossRef]
12. Cui, P.; Wang, W.; Nong, Z.; Lai, Z.; Liu, Y.; Zhu, J. Effects of Cr Content on Microstructure and Mechanical Properties of Co-Free $FeCryNiAl_{0.8}$ High-Entropy Alloys. *Materials* **2023**, *16*, 3348. [CrossRef]
13. Ye, Q.; Zhang, Z.; Wang, Q.; Xu, X.; Wang, K.; Zhao, J.; Xu, B.; Zhang, J.; Liu, D.; Deng, Y.; et al. Promoting nanoscale deformation twinning through FCC phase decomposition in $AlCoCrFeMo_{0.05}Ni_2$ high entropy alloy. *J. Alloys Compd.* **2024**, *985*, 174086. [CrossRef]
14. Li, D.; Liaw, P.K.; Xie, L.; Zhang, Y.; Wang, W. Advanced high-entropy alloys breaking the property limits of current materials. *J. Mater. Sci. Technol.* **2024**, *186*, 219–230. [CrossRef]
15. Liu, X.; Liu, H.; Wu, Y.; Li, M.; Xing, C.; He, Y. Tailoring phase transformation and precipitation features in a $Al_{21}Co_{19.5}Fe_{9.5}Ni_{50}$ eutectic high-entropy alloy to achieve different strength-ductility combinations. *J. Mater. Sci. Technol.* **2024**, *195*, 111–125. [CrossRef]
16. Cheng, J.C.; Li, N.; Huang, J.Y.; Cui, A.R.; Zhao, X.J.; Cai, Y.; Wang, Q.Y.; Luo, S.N. Dynamic compression responses of heterogeneous-structured CrMnFeCoNi high-entropy alloy at cryogenic temperatures. *Mater. Sci. Eng. A* **2024**, *892*, 146063. [CrossRef]
17. Stoian, A.B.; Nartita, R.; Totea, G.; Ionita, D.; Burnei, C. Complex Bioactive Chitosan–Bioglass Coatings on a New Advanced TiTaZrAg Medium–High-Entropy Alloy. *Coatings* **2023**, *13*, 971. [CrossRef]
18. Nartita, R.; Ionita, D.; Demetrescu, I.; Enachescu, M. A fresh perspective on medium entropy alloys applications as coating and coating substrate. *Ann. Acad. Rom. Sci. Ser. Phys. Chem.* **2022**, *7*, 34–46. [CrossRef]
19. Wu, Y.; Du, C.; Yu, Z.; Wang, R.; Ren, X. Effect of Cu content on the microstructure and mechanical properties of Fe20Co30Ni10Cr20Mn20 FCC-typed HEAs. *Mater. Sci. Eng. A* **2024**, *897*, 146336. [CrossRef]
20. Li, C.; Ma, Z.; Tong, S.; Liu, J.; Zhang, W.; Shen, G.; Wang, S.; Zhao, H.; Ren, L. Mechanical-thermal coupling fatigue failure of CoCrFeMnNi high entropy alloy. *J. Mater. Res. Technol.* **2024**, *30*, 3430–3437. [CrossRef]
21. Matsuzaka, T.; Hyakubu, A.; Kim, Y.S.; Matsugaki, A.; Nagase, T.; Ishimoto, T.; Ozasa, R.; Kim, H.S.; Mizuguchi, T.; Gokcekaya, O.; et al. Development of an equiatomic octonary TiNbTaZrMoHfWCr super-high-entropy alloy for biomedical applications. *Mater. Chem. Phys.* **2024**, *316*, 129120. [CrossRef]
22. Naveen, L.; Umre, P.; Chakraborty, P.; Rahul, M.R.; Samal, S.; Tewari, R. Development of single-phase BCC refractory high entropy alloys using machine learning techniques. *Comput. Mater. Sci.* **2024**, *238*, 112917. [CrossRef]
23. Wakai, E.; Noto, H.; Shibayama, T.; Furuya, K.; Ando, M.; Kamada, T.; Ishida, T.; Makimura, S. Microstructures and hardness of BCC phase iron-based high entropy alloy Fe-Mn-Cr-V-Al-C. *Mater. Charact.* **2024**, *211*, 113881. [CrossRef]
24. Yusenko, K.V.; Riva, S.; Crichton, W.A.; Spektor, K.; Bykova, E.; Pakhomova, A.; Tudball, A.; Kupenko, I.; Rohrbach, A.; Klemme, S.; et al. High-pressure high-temperature tailoring of High Entropy Alloys for extreme environments. *J. Alloys Compd.* **2018**, *738*, 491–500. [CrossRef]
25. Li, Y.; Wang, X.; Shi, Z.; Liang, J. Phase Structure, Microstructure, Corrosion, and Wear Resistance of $Al_{0.8}CrFeCoNiCu_{0.5}$ High-Entropy Alloy. *Lubricants* **2023**, *11*, 358. [CrossRef]
26. Huang, D.C.; Ran, X.X.; Cai, Y.; Liu, X.H.; Lu, L. Strain partitioning in dual-phase eutectic high-entropy alloy: Dependence on phase boundary morphology. *Scr. Mater.* **2024**, *247*, 116077. [CrossRef]
27. Li, G.; Li, Y.; Liang, J.; Wen, Z.; Zhang, T.; Ding, X.; Qu, Y. Influence of C14 Laves phase and Zr-rich phase interactions on the hydrogen storage properties of $Ti_{32.5}V_{27.5}Zr_{7.5}Nb_{32.5}$ high entropy hydrogen storage alloy. *Intermetallics* **2024**, *168*, 108239. [CrossRef]
28. Yusenko, K.V.; Riva, S.; Carvalho, P.A.; Yusenko, M.V.; Arnaboldi, S.; Sukhikh, A.S.; Hanfland, M.; Gromilov, S.A. First hexagonal close packed high-entropy alloy with outstanding stability under extreme conditions and electrocatalytic activity for methanol oxidation. *Scr. Mater.* **2017**, *138*, 22–27. [CrossRef]
29. Araujo, R.B.; Bayrak Pehlivan, I.; Edvinsson, T. High-entropy alloy catalysts: Fundamental aspects, promises towards electrochemical NH_3 production, and lessons to learn from deep neural networks. *Nano Energy* **2023**, *105*, 108027. [CrossRef]
30. Kumari, P.; Gupta, A.K.; Mishra, R.K.; Ahmad, M.S.; Shahi, R.R. A Comprehensive Review: Recent Progress on Magnetic High Entropy Alloys and Oxides. *J. Magn. Magn. Mater.* **2022**, *554*, 169142. [CrossRef]
31. Aidhy, D.S. Chemical randomness, lattice distortion and the wide distributions in the atomic level properties in high entropy alloys. *Comput. Mater. Sci.* **2024**, *237*, 112912. [CrossRef]

32. He, Z.; Jia, N.; Wang, H.; Yan, H.; Shen, Y. Synergy effect of multi-strengthening mechanisms in FeMnCoCrN HEA at cryogenic temperature. *J. Mater. Sci. Technol.* **2021**, *86*, 158–170. [CrossRef]
33. Ghosh, P.S.; Ali, K.; Arya, A. Efficient screening of single phase forming low-activation high entropy alloys. *J. Alloys Compd.* **2024**, *978*, 173172. [CrossRef]
34. Gludovatz, B.; Ritchie, R.O. Fracture properties of high-entropy alloys. *MRS Bull.* **2022**, *47*, 176–185. [CrossRef]
35. Shi, P.; Ren, W.; Zheng, T.; Ren, Z.; Hou, X.; Peng, J.; Hu, P.; Gao, Y.; Zhong, Y.; Liaw, P.K. Enhanced strength–ductility synergy in ultrafine-grained eutectic high-entropy alloys by inheriting microstructural lamellae. *Nat. Commun.* **2019**, *10*, 489. [CrossRef] [PubMed]
36. Nene, S.S.; Frank, M.; Agrawal, P.; Sinha, S.; Liu, K.; Shukla, S.; Mishra, R.S.; McWilliams, B.A.; Cho, K.C. Microstructurally flexible high entropy alloys: Linkages between alloy design and deformation behavior. *Mater. Des.* **2020**, *194*, 108968. [CrossRef]
37. Jiang, K.; Li, J.; Suo, T. Extensive phase transformation in an equiatomic CrCoNi medium entropy alloy under extreme uniaxial tension. *Int. J. Plast.* **2024**, *176*, 103968. [CrossRef]
38. Yoon, K.N.; Oh, H.S.; Kim, J.Y.; Kim, M.S.; Zhang, J.; Park, E.S. A new class of light-weight metastable high entropy alloy with high strength and large ductility. *Materialia* **2022**, *21*, 101284. [CrossRef]
39. Chen, W.; Li, X. Structure and mechanical properties of novel lightweight refractory high entropy alloys NbMoTiZr-(Al/V): A combined first principles and experimental study. *J. Alloys Compd.* **2024**, *973*, 172855. [CrossRef]
40. Basu, S.S.; Jana, P.P.; Ghosh, M. A new insight into the phase stability in high entropy alloys. *Mater. Today Commun.* **2023**, *37*, 107394. [CrossRef]
41. Balaji, V.; Xavior, A. Development of high entropy alloys (HEAs): Current trends. *Heliyon* **2024**, *10*, e26464. [CrossRef] [PubMed]
42. Jian, W.; Ren, L. Insights into orientation-dependent plasticity deformation of HfNbTaTiZr refractory high entropy alloy: An atomistic investigation. *Int. J. Plast.* **2024**, *173*, 103867. [CrossRef]
43. Kang, B.; Lee, S.; Lee, W.; Yoon, K.N.; Park, E.S.; Jang, H. Review on thermal transport and lattice dynamics of high-entropy alloys containing Ni. *Curr. Opin. Solid State Mater. Sci.* **2024**, *29*, 101146. [CrossRef]
44. Peng, J.; Li, J.; Mohammadzadeh, R. Role of lattice resistance in the shock dynamics of fcc-structured high entropy alloy. *Mater. Today Commun.* **2022**, *33*, 104884. [CrossRef]
45. Jiang, K.; Zhang, Q.; Li, J.; Li, X.; Zhao, F.; Hou, B.; Suo, T. Abnormal hardening and amorphization in an FCC high entropy alloy under extreme uniaxial tension. *Int. J. Plast.* **2022**, *159*, 103463. [CrossRef]
46. Li, R.; Xie, L.; Wang, W.Y.; Liaw, P.K.; Zhang, Y. High-Throughput Calculations for High-Entropy Alloys: A Brief Review. *Front. Mater.* **2020**, *7*, 290. [CrossRef]
47. Zhang, S.; Sun, Y.; Cheng, W.; Chen, Y.; Gu, J. High temperature oxidation behavior of $CoCrFeNiMo_{0.2}$ high-entropy alloy coatings produced by laser cladding. *Mater. Today Commun.* **2024**, *39*, 108639. [CrossRef]
48. Li, Y.; Bai, Y.; Liu, Z.; Jiang, Q.; Zhang, K.; Wei, B. Additive manufacturing-induced anisotropy in damping performance of a dual-phase high-entropy alloy. *J. Mater. Res. Technol.* **2024**, *29*, 5752–5764. [CrossRef]
49. Qin, Y.; Wang, Y.; Guan, S.; Wang, C.; Jiang, B.; Wang, W.; Huang, M.; Peng, B.; Li, Q.; Peng, F.; et al. High-pressure preparation of high-hardness $CoCrFeNiMo_{0.4}$ high-entropy alloy. *Int. J. Refract. Met. Hard Mater.* **2022**, *102*, 105718. [CrossRef]
50. Lan, Y.; Zhang, Y.; Peng, Y.; Wang, A.; Gao, Y.; Yang, W.; Fan, W.; Zhang, W.; Liu, Y. In-situ synthesis of dual-phase nitrides and multiple strengthening mechanisms in $FeCoCrNiA_{l0.5}$ high entropy matrix composite coatings by laser cladding and plasma nitriding. *J. Alloys Compd.* **2024**, *990*, 174400. [CrossRef]
51. Verma, P.K.; Singh, A.; Kumar, A. Microstructure characterization and phase evolution of equiatomic AlCoMoFeNi high entropy alloy synthesized by mechanical alloying. *Mater. Chem. Phys.* **2024**, *318*, 129325. [CrossRef]
52. Yan, P.X.; Chang, J.; Wang, W.L.; Zhu, X.N.; Lin, M.J.; Wei, B. Metastable phase separation and crystalline orientation feature of electromagnetic levitation processed CoCrCuFeNi high entropy alloy. *Acta Mater.* **2024**, *269*, 119778. [CrossRef]
53. Salifu, S.; Olubambi, P.A.; Teffo, L. Phase stability and microstructural properties of high entropy alloy reinforced aluminium matrix composites consolidated via spark plasma sintering. *Heliyon* **2024**, *10*, e24498. [CrossRef] [PubMed]
54. Meghwal, A.; Pinches, S.; Anupam, A.; Lie, L.; Munroe, P.; Berndt, C.C.; Siao Ming Ang, A. Structure-property correlation of a CoCrFeNi medium-entropy alloy manufactured using extreme high-speed laser material deposition (EHLA). *Intermetallics* **2023**, *152*, 107769. [CrossRef]
55. Zhou, J.L.; Cheng, Y.H.; Wan, Y.X.; Chen, H.; Wang, Y.F.; Yang, J.Y. Strengthening by Ti, Nb, and Zr doping on microstructure, mechanical, tribological, and corrosion properties of CoCrFeNi high-entropy alloys. *J. Alloys Compd.* **2024**, *984*, 173819. [CrossRef]
56. Toroghinejad, M.R.; Pirmoradian, H.; Shabani, A. Synthesis of FeCrCoNiCu high entropy alloy through mechanical alloying and spark plasma sintering processes. *Mater. Chem. Phys.* **2022**, *289*, 126433. [CrossRef]
57. Straumal, B.B.; Klinger, L.; Kuzmin, A.; Lopez, G.A.; Korneva, A.; Straumal, A.B.; Vershinin, N.; Gornakova, A.S. High Entropy Alloys Coatings Deposited by Laser Cladding: A Review of Grain Boundary Wetting Phenomena. *Coatings* **2022**, *12*, 343. [CrossRef]
58. Onawale, O.T.; Cobbinah, P.V.; Nzeukou, R.A.; Matizamhuka, W.R. Synthesis Route, Microstructural Evolution, and Mechanical Property Relationship of High-Entropy Alloys (HEAs): A Review. *Materials* **2021**, *14*, 3065. [CrossRef] [PubMed]

59. Sonar, T.; Ivanov, M.; Trofimov, E.; Tingaev, A.; Suleymanova, I. An overview of microstructure, mechanical properties and processing of high entropy alloys and its future perspectives in aeroengine applications. *Mater. Sci. Energy Technol.* **2024**, *7*, 35–60. [CrossRef]
60. Zhang, W.; Shen, J.; Oliveira, J.P.; Kooi, B.J.; Pei, Y. Crystallographic orientation-dependent deformation characteristics of additive manufactured interstitial-strengthened high entropy alloys. *Scr. Mater.* **2023**, *222*, 115049. [CrossRef]
61. Yang, Z.; Fu, B.; Ning, Z.; Bai, X.; Yang, H.; Chen, Q.; Luo, D.; Qiu, N.; Wang, Y. Amorphization activated by semicoherent interfaces of FCC/BCC HEA multilayers during deformation. *Mater. Des.* **2023**, *225*, 111469. [CrossRef]
62. Li, K.; Zhai, Y.; Lai, M.; Song, M.; Zou, S.; Huang, G.; Yaqoob, K.; Wang, Z.; Zhang, N. Corrosion of Eutectic High-Entropy Alloys: A Review. *Crystals* **2023**, *13*, 1231. [CrossRef]
63. Yang, Z.; Qiu, N.; Yang, H.; Chen, Q.; Wang, Y. Irradiation tolerance enhanced by coherent interfaces of FCC/BCC HEA multilayers. *Surf. Coat. Technol.* **2023**, *457*, 129338. [CrossRef]
64. Liu, J.; Li, Z.; Lin, D.; Tang, Z.; Song, X.; He, P.; Zhang, S.; Bian, H.; Fu, W.; Song, Y. Eutectic high-entropy alloys and their applications in materials processing engineering: A review. *J. Mater. Sci. Technol.* **2024**, *189*, 211–246. [CrossRef]
65. Zhang, Q.; Chen, Z.; Dong, Y.; Li, C.; Wang, Y. High strength and ductility eutectic high entropy alloy with unique core-shell structure. *J. Alloys Compd.* **2024**, *976*, 173141. [CrossRef]
66. Xiao, L.; Feng, J.; Pan, W.; Zhang, G.; Yue, P.; Yang, S. Extreme thermal stability in crystal-amorphous nanocrystalline CoCrFeMnNi high entropy alloy. *Mater. Lett.* **2023**, *352*, 135206. [CrossRef]
67. Siddique, A.; Abid, T.; Akram, M.A.; Bin Yaqub, T.; Karim, M.R.A.; Fernandes, F.; Khan, R.; Yaqoob, K. Design and development of NbTiVZr porous high entropy alloys for energy applications. *J. Energy Storage* **2023**, *73*, 109131. [CrossRef]
68. Liu, G.; Li, S.; Song, C.; Liu, Z.; Du, J.; Xie, X.; Wang, Y.; Cong, D. High-entropy Ti-Zr-Hf-Ni-Cu alloys as solid-solid phase change materials for high-temperature thermal energy storage. *Intermetallics* **2024**, *166*, 108177. [CrossRef]
69. Yoshizaki, T.; Fujita, T. Thermal stability and phase separation of nanoporous high-entropy alloys containing 23 elements. *J. Alloys Compd.* **2023**, *968*, 172056. [CrossRef]
70. Nitol, M.S.; Echeverria, M.J.; Dang, K.; Baskes, M.I.; Fensin, S.J. New modified embedded-atom method interatomic potential to understand deformation behavior in VNbTaTiZr refractory high entropy alloy. *Comput. Mater. Sci.* **2024**, *237*, 112886. [CrossRef]
71. Ren, H.; Chen, R.R.; Gao, X.F.; Liu, T.; Qin, G.; Wu, S.P.; Guo, J.J. High-performance AlCoCrFeNi high entropy alloy with marine application perspective. *J. Mater. Res. Technol.* **2023**, *25*, 6751–6763. [CrossRef]
72. Ionita, D.; Pirvu, C.; Stoian, A.B.; Demetrescu, I. The Trends of TiZr Alloy Research as a Viable Alternative for Ti and $Ti_{16}Zr$ Roxolid Dental Implants. *Coatings* **2020**, *10*, 422. [CrossRef]
73. Pantazi, A.; Vardaki, M.; Mihai, G.; Ionita, D.; Stoian, A.B.; Enachescu, M.; Demetrescu, I. Understanding surface and interface properties of modified $Ti_{50}Zr$ with nanotubes. *Appl. Surf. Sci.* **2020**, *506*, 144661. [CrossRef]
74. Mazare, A.; Totea, G.; Burnei, C.; Schmuki, P.; Demetrescu, I.; Ionita, D. Corrosion, antibacterial activity and haemocompatibility of TiO_2 nanotubes as a function of their annealing temperature. *Corros. Sci.* **2016**, *103*, 215–222. [CrossRef]
75. Berger, J.E.; Jorge, A.M.; Asato, G.H.; Roche, V. Formation of self-ordered oxide nanotubes layer on the equiatomic TiNbZrHfTa high entropy alloy and bioactivation procedure. *J. Alloys Compd.* **2021**, *865*, 158837. [CrossRef]
76. Bi, D.; Chang, Y.; Luo, H.; Pan, Z.; Zhao, Q.; Cheng, H.; Wang, X.; Qiao, C.; Ni, Z.; Liu, A.; et al. Corrosion behavior and passive film characteristics of $AlNbTiZrSi_x$ high-entropy alloys in simulated seawater environment. *Corros. Sci.* **2023**, *224*, 111530. [CrossRef]
77. Tunes, M.A.; Fritze, S.; Osinger, B.; Willenshofer, P.; Alvarado, A.M.; Martinez, E.; Menon, A.S.; Ström, P.; Greaves, G.; Lewin, E.; et al. From high-entropy alloys to high-entropy ceramics: The radiation-resistant highly concentrated refractory carbide (CrNbTaTiW)C. *Acta Mater.* **2023**, *250*, 118856. [CrossRef]
78. Huang, S.; Zhang, J.; Fu, H.; Xiong, Y.; Ma, S.; Xiang, X.; Xu, B.; Lu, W.; Zhang, Y.; Weber, W.J.; et al. Irradiation performance of high entropy ceramics: A comprehensive comparison with conventional ceramics and high entropy alloys. *Prog. Mater. Sci.* **2024**, *143*, 101250. [CrossRef]
79. Qi, Y.; Xu, H.; He, T.; Feng, M. Effect of crystallographic orientation on mechanical properties of single-crystal CoCrFeMnNi high-entropy alloy. *Mater. Sci. Eng. A* **2021**, *814*, 141196. [CrossRef]
80. Liu, B.; Jian, Z.; Guo, L.; Li, X.; Wang, K.; Deng, H.; Hu, W.; Xiao, S.; Yuan, D. Effect of crystallographic orientations on shock-induced plasticity for CoCrFeMnNi high-entropy alloy. *Int. J. Mech. Sci.* **2022**, *226*, 107373. [CrossRef]
81. Ashby, M.F.; Cebon, D. Materials selection in mechanical design. *Le J. Phys. IV* **1993**, *3*, C7-1–C7-9. [CrossRef]
82. Ashby, M.F. *Materials and Sustainable Development*; Elsevier: Amsterdam, The Netherlands, 2023; ISBN 9780323983617.
83. Chakraborty, P.; Sarkar, A.; Ali, K.; Jha, J.; Jothilakshmi, N.; Arya, A.; Tewari, R. Design and development of low density, high strength ZrNbAlVTi high entropy alloy for high temperature applications. *Int. J. Refract. Met. Hard Mater.* **2023**, *113*, 106222. [CrossRef]
84. Yang, H.; Shao, Z.; Lu, Q.; Cui, C.; Xu, L.; Yang, G. Development of reduced-activation and radiation-resistant high-entropy alloys for fusion reactor. *Int. J. Refract. Met. Hard Mater.* **2024**, *121*, 106674. [CrossRef]
85. Gawel, R.; Rogal, Ł.; Smoła, G.; Grzesik, Z. High-temperature oxidation and diffusion studies on selected Al–Cr–Fe–Ni high-entropy alloys for potential application in thermal barrier coatings. *Intermetallics* **2024**, *169*, 108273. [CrossRef]

86. Güler, S.H.; Güler, Ö.; Kavaz, E.; Almisned, G.; Issa, B.; Tekin, H.O. Exploring critical behavioral differences in physical, structural, and nuclear radiation attenuation properties of produced High Entropy Alloy (HEA) and Refractory-High Entropy Alloy (RHEA) samples. *Curr. Appl. Phys.* **2024**, *58*, 1–10. [CrossRef]
87. Golgovici, F.; Tudose, A.E.; Diniasi, D.; Nartita, R.; Fulger, M.; Demetrescu, I. Aspects of Applied Chemistry Related to Future Goals of Safety and Efficiency in Materials Development for Nuclear Energy. *Molecules* **2023**, *28*, 874. [CrossRef]
88. Zareipour, F.; Shahmir, H.; Huang, Y. Formation and significance of topologically close-packed Laves phases in refractory high-entropy alloys. *J. Alloys Compd.* **2024**, *986*, 174148. [CrossRef]
89. Kalita, D.; Jóźwik, I.; Kurpaska, Ł.; Zhang, Y.; Mulewska, K.; Chrominski, W.; O'Connell, J.; Ge, Y.; Boldman, W.L.; Rack, P.D.; et al. The microstructure and He^+ ion irradiation behavior of novel low-activation W-Ta-Cr-V refractory high entropy alloy for nuclear applications. *Nucl. Mater. Energy* **2023**, *37*, 101513. [CrossRef]
90. Li, P.; Zhang, J.; Yang, T.; Zhang, T.; Zhang, J.; Lin, J.; Yan, Y.; Li, C.; Si, X.; Cao, J.; et al. Characteristics, applications and perspective of high entropy alloys for interfacial joining: A review. *J. Manuf. Process.* **2024**, *110*, 303–317. [CrossRef]
91. Senkov, O.N.; Miracle, D.B.; Rao, S.I. Correlations to improve room temperature ductility of refractory complex concentrated alloys. *Mater. Sci. Eng. A* **2021**, *820*, 141512. [CrossRef]
92. Tunes, M.A.; Vo, H.T.; Baldwin, J.K.S.; Saleh, T.A.; Fensin, S.J.; El-Atwani, O. Perspectives on novel refractory amorphous high-entropy alloys in extreme environments. *Appl. Mater. Today* **2023**, *32*, 101796. [CrossRef]
93. Senkov, O.N.; Gorsse, S.; Miracle, D.B. High temperature strength of refractory complex concentrated alloys. *Acta Mater.* **2019**, *175*, 394–405. [CrossRef]
94. Wang, F.; Yang, T.; Zhong, Y.; Li, L.; Yuan, T. Design crystallographic ordering in $NbTa_{0.5}TiAl_x$ refractory high entropy alloys with strength-plasticity synergy. *J. Mater. Res. Technol.* **2023**, *27*, 8386–8402. [CrossRef]
95. Xu, Z.Q.; Ma, Z.L.; Wang, M.; Chen, Y.W.; Tan, Y.D.; Cheng, X.W. Design of novel low-density refractory high entropy alloys for high-temperature applications. *Mater. Sci. Eng. A* **2019**, *755*, 318–322. [CrossRef]
96. Yu, K.; Cheng, J.; Cheng, Q.; Geng, Y.; Zhu, S.; Liu, M.; Wan, S.; Yang, J. Enhanced wear resistance in (CoCrNi)94Al3Ti3 medium-entropy alloy at high temperatures via nano-Al_2O_3 reinforcing phase. *Tribol. Int.* **2024**, *195*, 109569. [CrossRef]
97. Hu, J.C.; Yang, K.; Wang, Q.Y.; Zhao, Q.C.; Jiang, Y.H.; Liu, Y.J. Ultra-long life fatigue behavior of a high-entropy alloy. *Int. J. Fatigue* **2024**, *178*, 108013. [CrossRef]
98. Jenczyk, P.; Jarzabek, D.M.; Lu, Z.; Gadalińska, E.; Levintant-Zayonts, N.; Zhang, Y. Unexpected crystallographic structure, phase transformation, and hardening behavior in the $AlCoCrFeNiTi_{0.2}$ high-entropy alloy after high-dose nitrogen ion implantation. *Mater. Des.* **2022**, *216*, 110568. [CrossRef]
99. Ganesh Reddy Majji, B.; Vasudev, H.; Bansal, A. Application of plasma-sprayed $Al_xCrCoFeNi$ High-Entropy alloys for high-temperature oxidation resistance. *Mater. Lett.* **2024**, *361*, 136069. [CrossRef]
100. Kwon, H.J.; Lim, K.R.; Kim, Y.K.; Na, Y.S.; Yi, S. Design strategy for high-entropy alloys with enhanced microstructural stability and mechanical properties for high-temperature applications. *Mater. Sci. Eng. A* **2024**, *889*, 145836. [CrossRef]
101. Kumar, A.; Abu, M.; Krishna, N.; Yadav, P. Phase transformation of AB 5 to AB 2 type phase on substitution of Mn with Zr in TiVCoNi (Zr_xMn_{2-x}) (x = 0, 0.3, 0.6, 1.0) high entropy alloys. *Mater. Chem. Phys.* **2024**, *318*, 129291. [CrossRef]
102. Shen, J.; Hu, J.; An, X. Regulation of phase partition and wear resistance for FeCoCrV high entropy alloy by heat treatment. *Intermetallics* **2024**, *167*, 108232. [CrossRef]
103. Yang, Z.; Qiu, N.; Yang, H.; Wang, Y. Vacancies-mediated atomic diffusion controlled by the interfacial structure of FCC/BCC HEA multilayers. *J. Alloys Compd.* **2023**, *947*, 169512. [CrossRef]
104. Anamu, U.S.; Ayodele, O.O.; Olorundaisi, E.; Babalola, B.J.; Odetola, P.I.; Ogunmefun, A.; Ukoba, K.; Jen, T.C.; Olubambi, P.A. Fundamental design strategies for advancing the development of high entropy alloys for thermo-mechanical application: A critical review. *J. Mater. Res. Technol.* **2023**, *27*, 4833–4860. [CrossRef]
105. Zhang, S.X.; Huang, X.M.; Cai, G.M. The strategy of design and preparation for outstanding precipitation strengthened HEAs based on diffusion couple. *Mater. Des.* **2022**, *217*, 110667. [CrossRef]
106. Charkhchian, J.; Zarei-Hanzaki, A.; Moshiri, A.; Schwarz, T.M.; Lawitzki, R.; Schmitz, G.; Schell, N.; Shen, J.; Oliveira, J.P.; Waryoba, D.; et al. Unraveling the formation of $L1_2$ nano-precipitates within the FCC-phase in $AlCoCrFeNi_{2.1}$ eutectic high entropy alloy. *Vacuum* **2024**, *221*, 112919. [CrossRef]
107. Dastanpour, E.; Huang, S.; Ström, V.; Varga, L.K.; Vitos, L.; Schönecker, S. An assessment of the $Al_{50}Cr_{21-x}Mn_{17+x}Co_{12}$ (x = 0, 4, 8) high-entropy alloys for magnetocaloric refrigeration application. *J. Alloys Compd.* **2024**, *984*, 173977. [CrossRef]
108. Için, K. Investigation of phase transformation related magnetic properties of Ti addition to FeCoCuNiMn and FeCoCuNiAl high entropy alloys by vacuum arc melting. *Mater. Today Commun.* **2024**, *39*, 108821. [CrossRef]
109. Brodie, J.; Wang, J.; Couzinié, J.P.; Heczko, M.; Mazánová, V.; Mills, M.J.; Ghazisaeidi, M. Stability of the B2 phase in refractory high entropy alloys containing aluminum. *Acta Mater.* **2024**, *268*, 119745. [CrossRef]
110. He, Z.; Zhang, H.; Cheng, H.; Ge, M.; Si, T.; Che, L.; Zheng, K.; Zeng, L.; Wang, Q. Machine learning guided BCC or FCC phase prediction in high entropy alloys. *J. Mater. Res. Technol.* **2024**, *29*, 3477–3486. [CrossRef]
111. Chen, C.; Han, X.; Zhang, Y.; Liaw, P.K.; Ren, J. Phase prediction of high-entropy alloys based on machine learning and an improved information fusion approach. *Comput. Mater. Sci.* **2024**, *239*, 112976. [CrossRef]
112. Guo, Q.; Xu, X.; Pei, X.; Duan, Z.; Liaw, P.K.; Hou, H.; Zhao, Y. Predict the phase formation of high-entropy alloys by compositions. *J. Mater. Res. Technol.* **2023**, *22*, 3331–3339. [CrossRef]

113. Shen, L.; Chen, L.; Huang, J.; He, J.; Li, Z.; Pan, J.; Chang, F.; Dai, P.; Tang, Q. Predicting phases and hardness of high entropy alloys based on machine learning. *Intermetallics* **2023**, *162*, 108030. [CrossRef]
114. Yin, K.X.; Huang, Z.W.; Wu, B.L.; Zhang, G.J.; Tian, Q.W.; Wang, Y.N. Prediction of phase stabilities of solid solutions for high entropy alloys. *Acta Mater.* **2024**, *263*, 119445. [CrossRef]